Supporting Information

Enhanced Rate Performance of Lithium-Ion Battery Anodes Using Cobalt Incorporated Carbon Conductive Agent

Daubry Albert Claude Jean-Pierre[1†], Zhuijun Xu[2, 3†], Ming Yang[2], Ya-Jun Cheng[2*], Yonggao Xia[2,4], Xile Hu[1*]

1. Laboratory of Inorganic Synthesis and Catalysis, Institute of Chemical Sciences and Engineering, Ecole Polytechnique Fédérale de Lausanne (EPFL), ISIC-LSCI, BCH 3305, Lausanne 1015, Switzerland

2. Ningbo Institute of Materials Technology & Engineering, Chinese Academy of Sciences, 1219 Zhongguan West Rd, Zhenhai District, Ningbo, Zhejiang Province 315201 P. R. China

3. University of Chinese Academy of Sciences, 19A Yuquan Rd, Shijingshan District, Beijing 100049, People's Republic of China

4. Center of Materials Science and Optoelectronics Engineering, University of Chinese Academy of Sciences, 19A Yuquan Rd, Shijingshan District, Beijing 100049, P. R. China

† D.A. C. Jean-Pierre and Z. Xu contributed equally to this work.

E-mail: chengyj@nimte.ac.cn, and xile.hu@epfl.ch

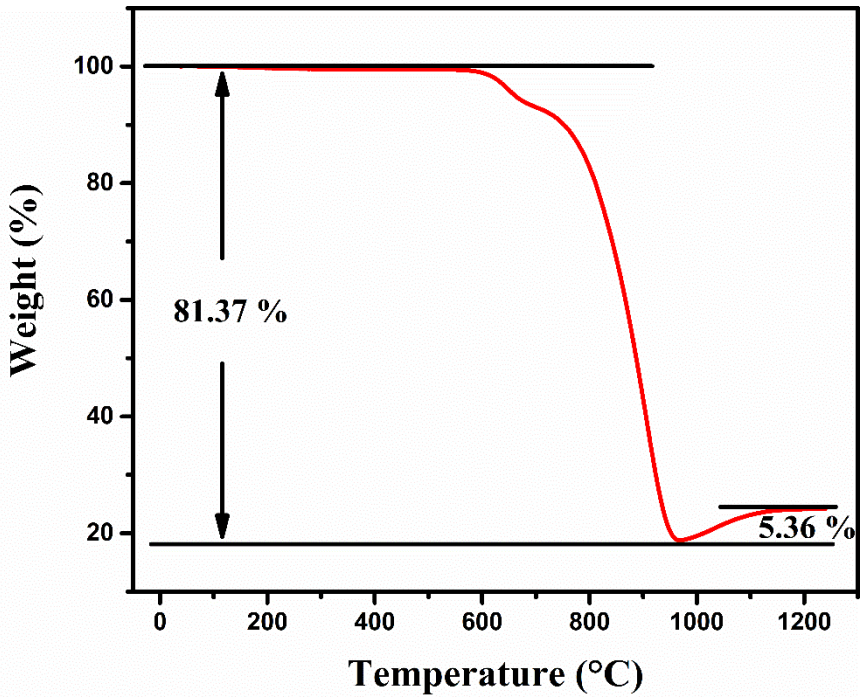

Figure S1. TG Curves of the Si/C composite anode material.

Thermogravimetric analysis (TGA) has been applied to measure the contents of silicon and graphite in the composite. As shown in Figure S1, a significant mass loss starts at around 650 °C accompanied by a 5.36 wt% mass increase near to 1000 °C. The mass loss from 650 °C to 1000 °C originates from the oxidation of the graphite component. The mass increase at 1000 °C is ascribed to the oxidation process of the silicon nanoparticles. If the end product after 1000 °C is assumed to be SiO_2, the graphite content is derived to be 89 wt% together with 11 wt% of silicon. Therefore, the theoretical specific capacity of Si /C composite anode material is 793 mAh g^{-1} (theoretical specific capacity of Si is 4200 mAh g^{-1} and theoretical specific capacity of graphite is 372 mAh g^{-1}).

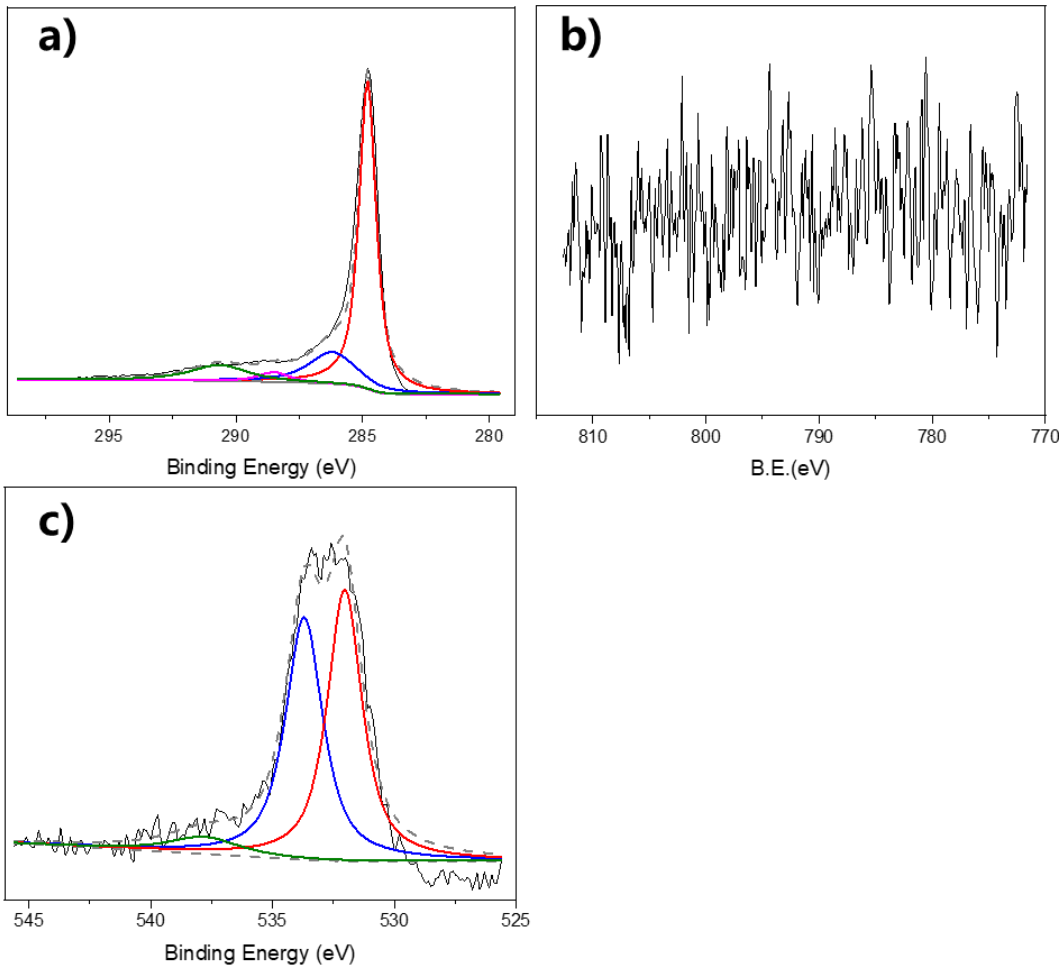

Figure S2. a-c) High resolution XPS spectra for C, Co and O of Co-ox-KJB, respectively.

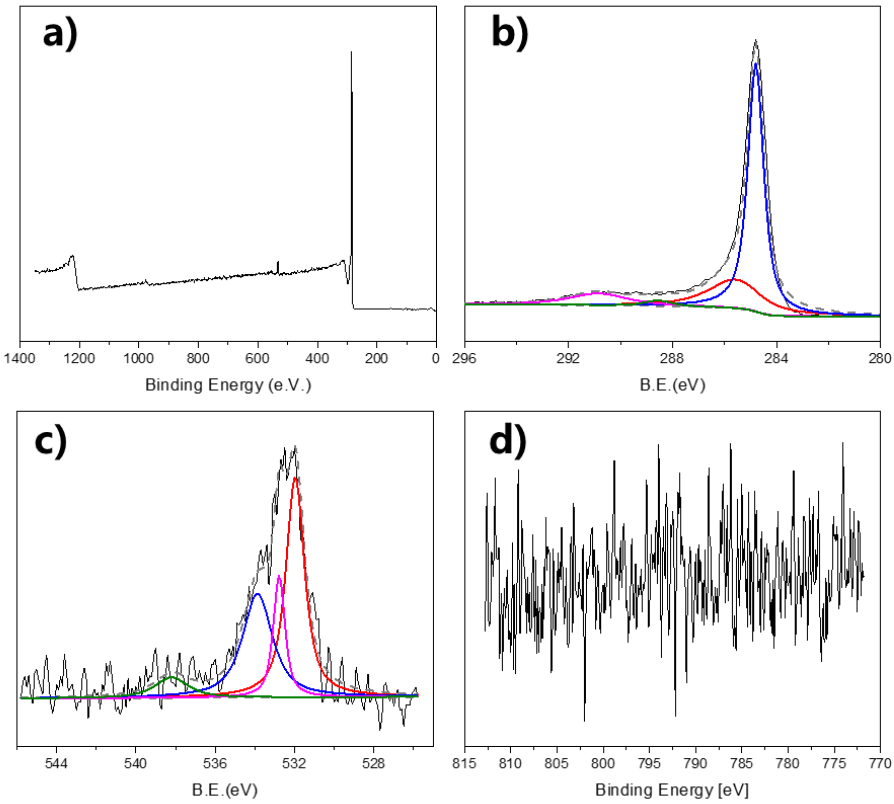

Figure S3. a) XPS spectra for KJB. b-d) High resolution XPS spectra for C, O and Co of KJB, respectively.

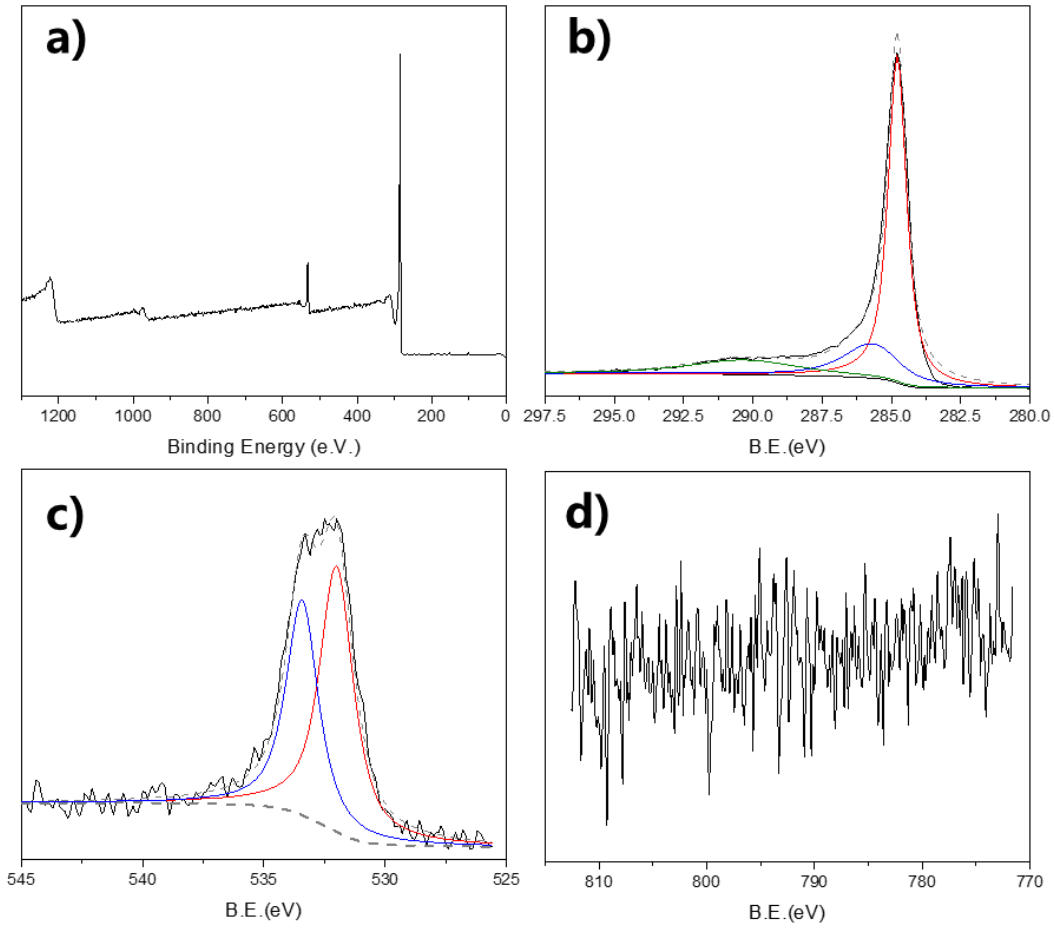

Figure S4. a) XPS spectra for ox-KJB. b-d) High resolution XPS spectra for C, O and Co of ox-KJB, respectively.

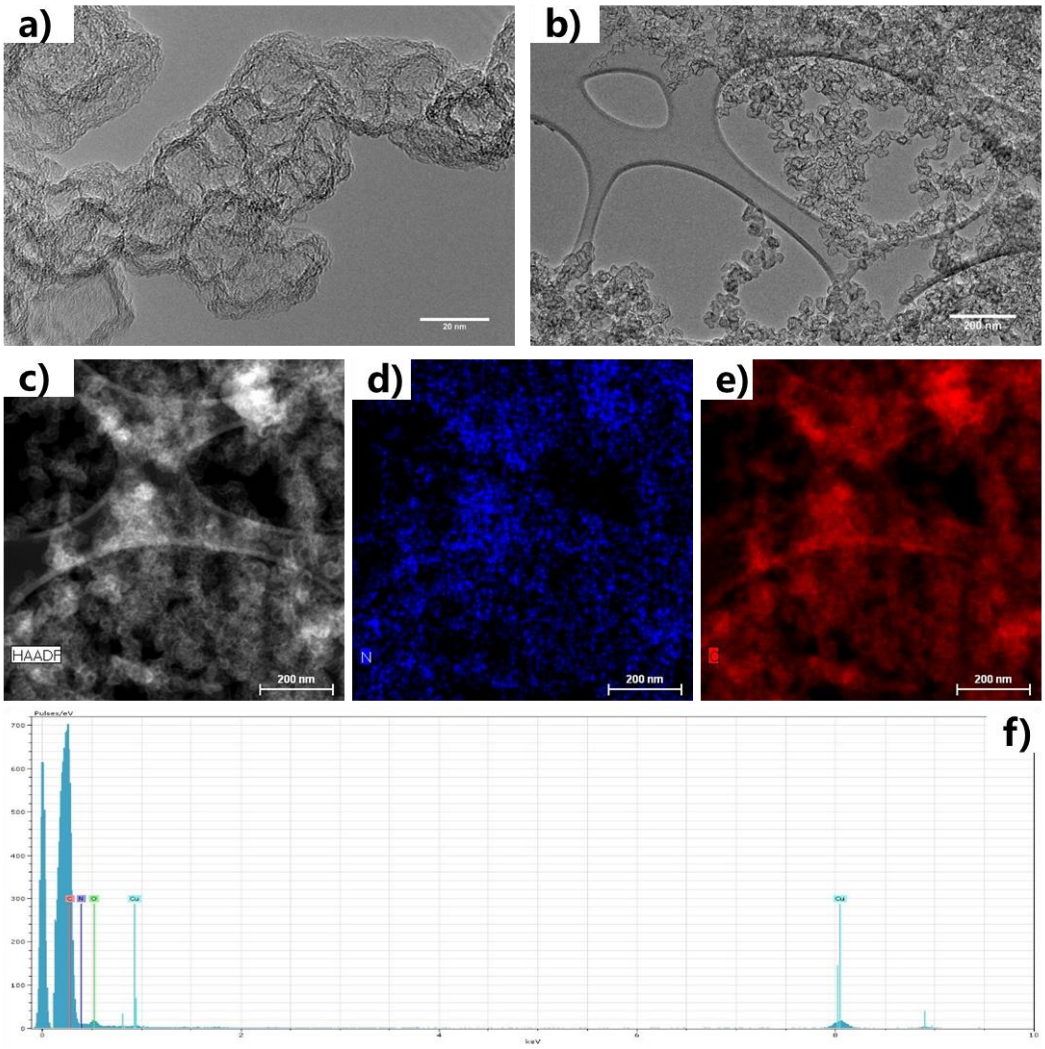

Figure S5. a-b) TEM images of KJB. c) HADDF images of KJB. d-e) EDS element mapping showing the distribution of C and O of KJB, respectively f) EDX image of KJB.

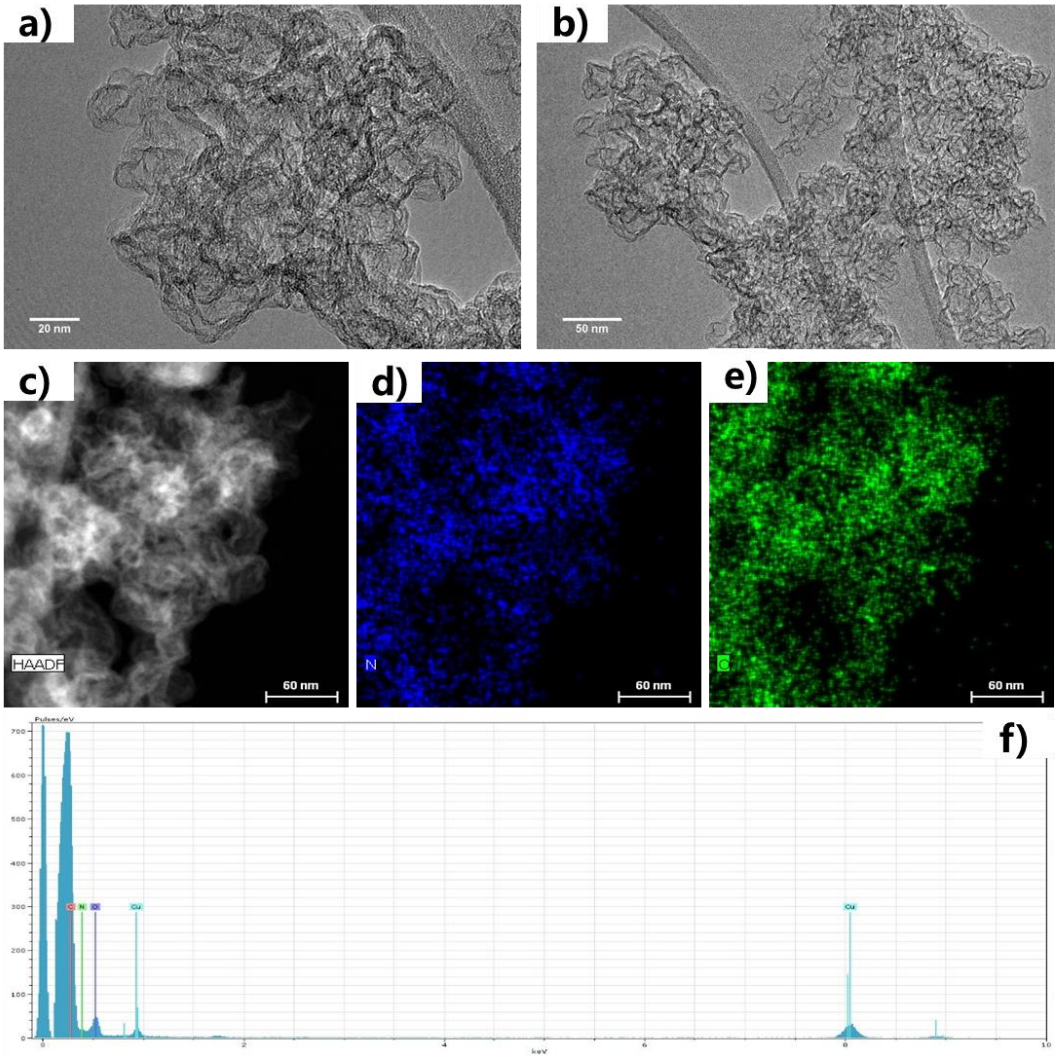

Figure S6. a-b) TEM images of ox-KJB. c) HADDF images of ox-KJB. d-e) EDS element mapping showing the distribution of C and O of ox-KJB, respectively. f) EDX image of ox-KJB.

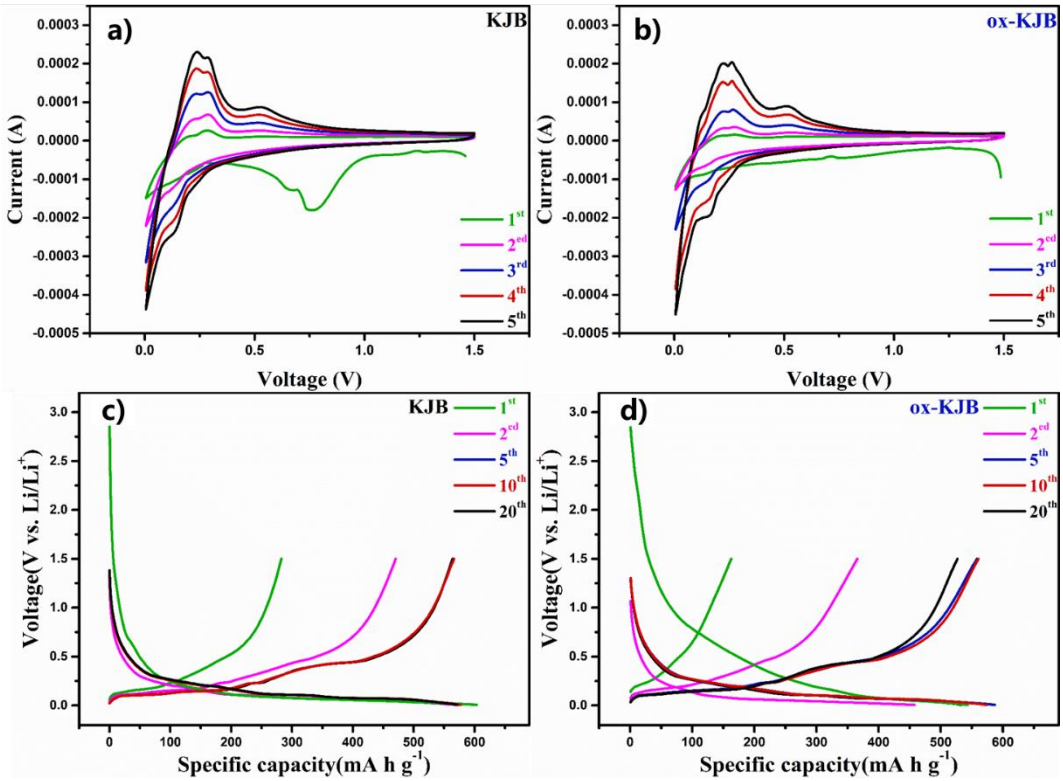

Figure S7. a-b) CV curves of pristine KJB and ox-KJB. c-d) Discharge and charge curves of pristine KJB and ox-KJB at 0.05 A g^{-1}.

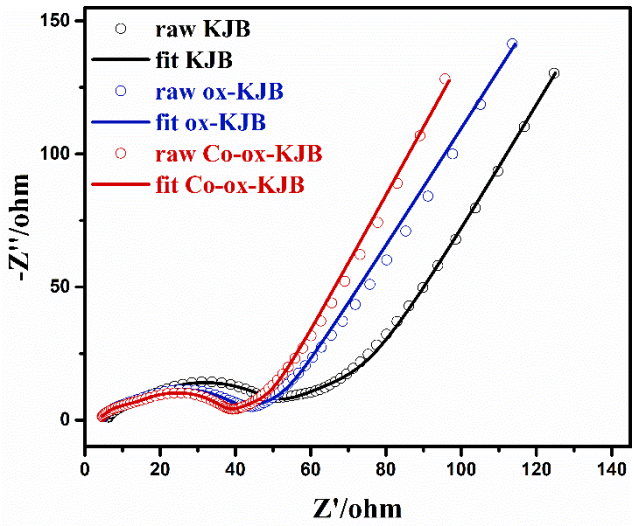

Figure S8. EIS curves of pristine KJB, ox-KJB and Co-ox-KJB after 10 cycles at 0.2 C (100 mA g^{-1}).

Table S1. Representative fitting data of EIS of the KJB, ox-KJB and Co-ox-KJB.

Sample	R_s (Ω)	R_{sei} (Ω)	R_{ct} (Ω)	R_{total} (Ω)
KJB	5.775	6.991	32.44	45.206
ox-KJB	4.180	7.610	26.39	38.180
Co-ox-KJB	3.879	9.82	21.57	35.269

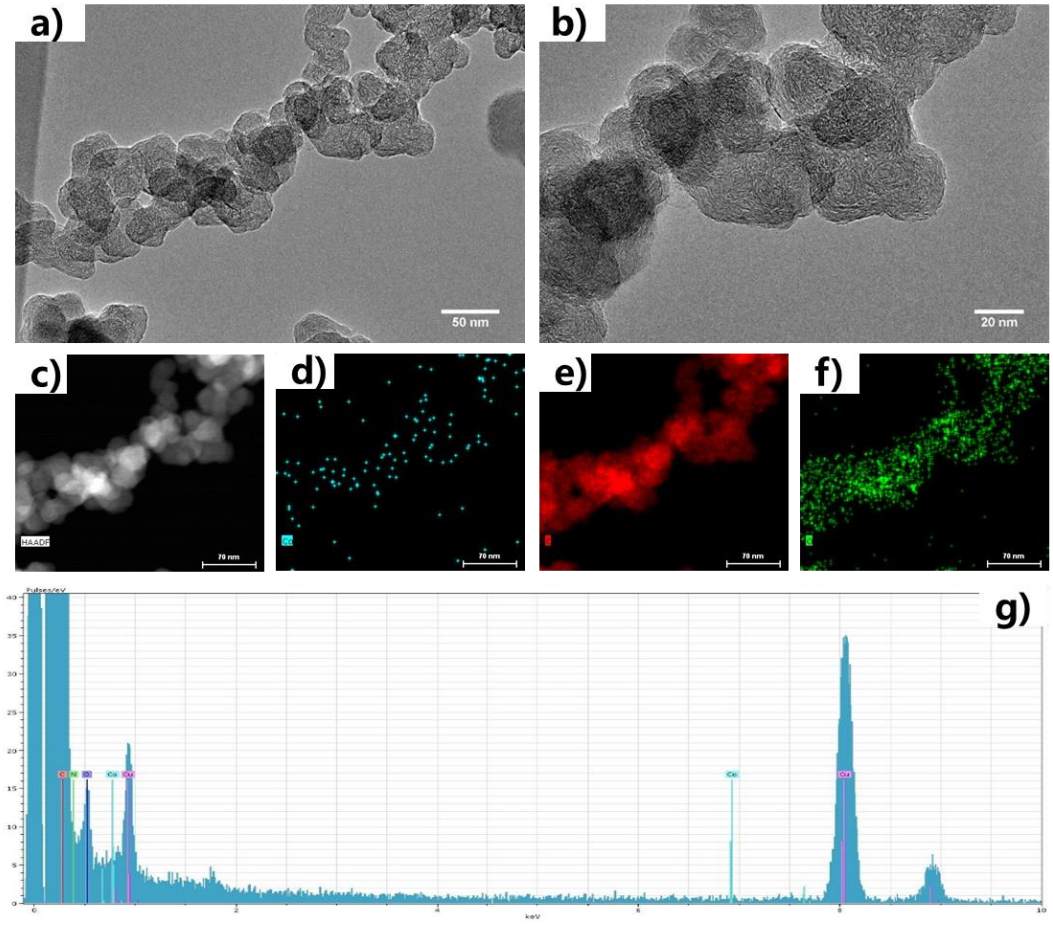

Figure S9. a-b) TEM images of Co-ox-super P. c) HADDF images of Co-ox-super P. d-f) EDS element mapping showing the distribution of Co, C and O of Co-ox-super P, respectively. g) EDX image of Co-ox-super P.

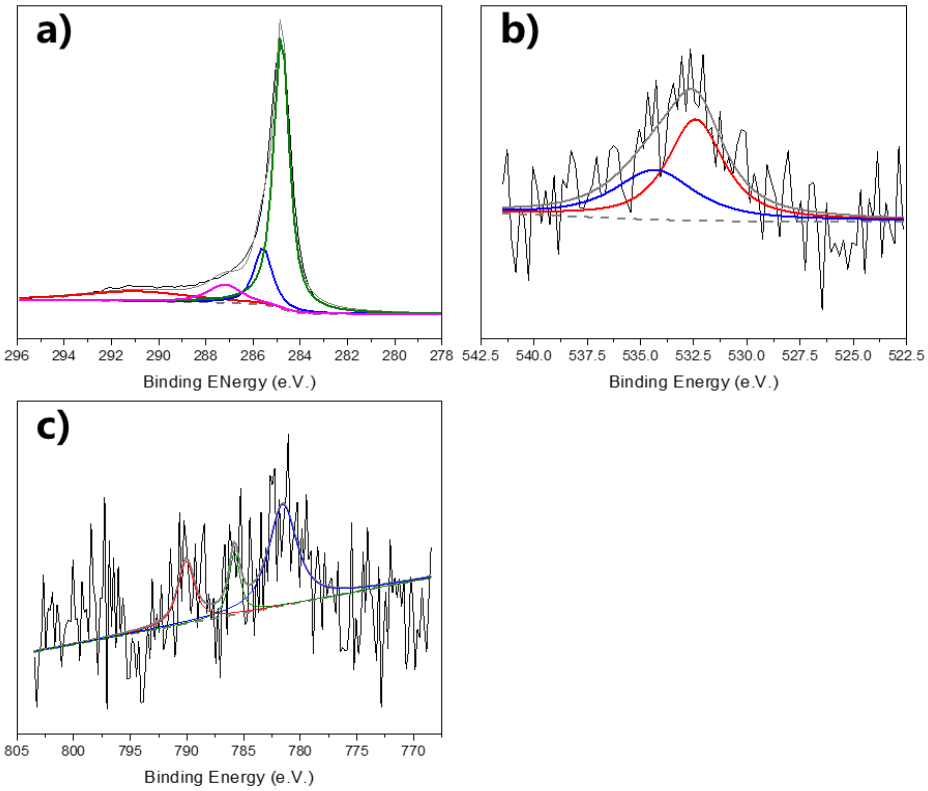

Figure S10. a-d) High resolution XPS spectra for C, O and Co of Co-ox-super P, respectively.

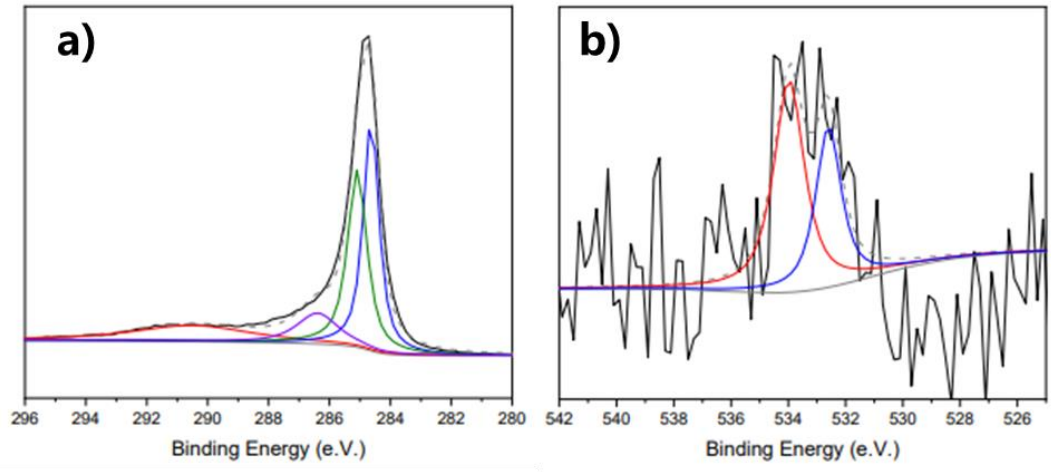

Figure S11. a-c) High resolution XPS spectra for C and O of super P, respectively.

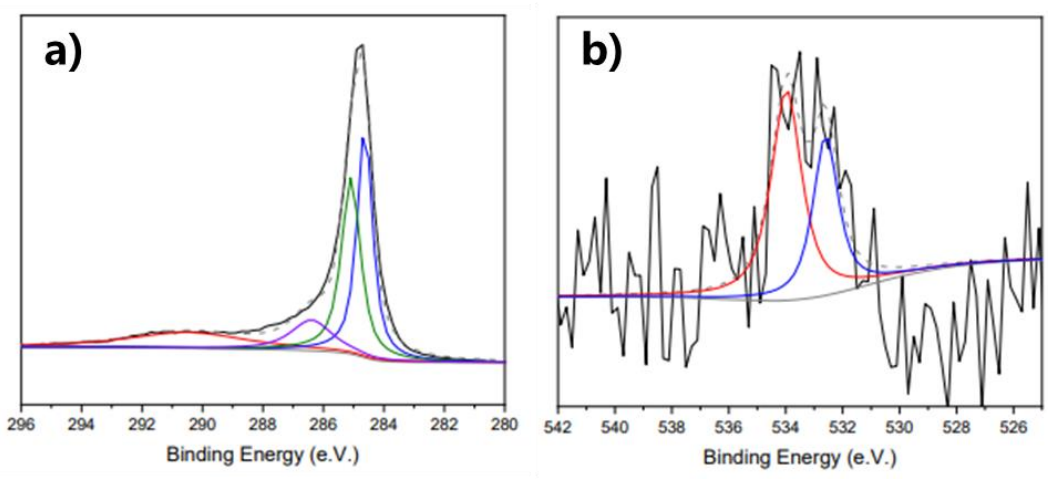

Figure S12. a-c) High resolution XPS spectra for C, O and N of ox-super P, respectively.

Table S2. average discharge capacity of the Si/C electrode with Pristine super P, ox-super P and Co-ox-super P during rate performance

	average discharge capacity of 5 cycles at different current density (mAh g^{-1})						
	0.05 A g^{-1}	0.1 A g^{-1}	0.25 A g^{-1}	0.5 A g^{-1}	1.0 A g^{-1}	1.5 A g^{-1}	0.1 A g^{-1}
super P	455	474	407	306	199	149	465
ox-super P	410	631	544	460	347	181	569
Co-ox-super P	472	662	570	487	378	209	575

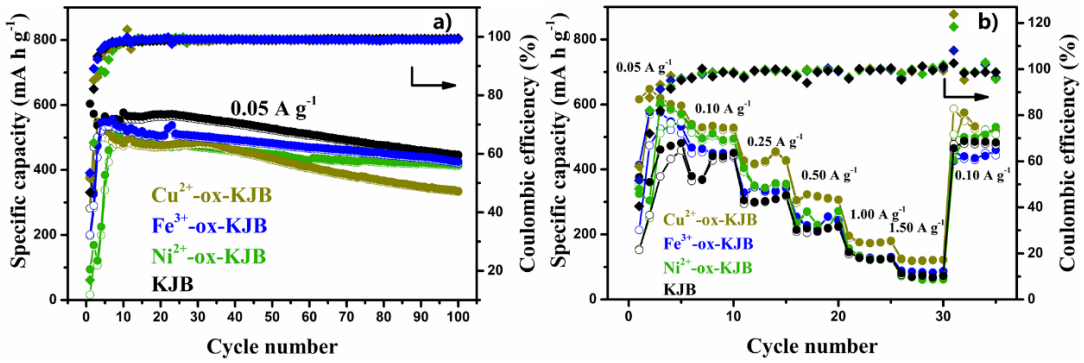

Figure S13. a) Long-term cycling performance at 50 mA g^{-1} of Cu^{2+}-ox-KJB (dark yellow), Fe^{3+}-ox-KJB (blue), Ni^{2+}-ox-KJB (green) and KJB (black). d) Rate capability test from 0.05 A g^{-1} to 1.50 A g^{-1}, followed by returning to 0.10 A g^{-1} with 5 cycles of Cu^{2+}-ox-KJB (dark yellow), Fe^{3+}-ox-KJB (blue), Ni^{2+}-ox-KJB (green) and KJB (black).

The incorporation of Cu, Fe, and Ni does not show as good a performance as cobalt. As the metallic species are incorporated into the Ketjen black in the form of nitrate salts, the metal ions tend to be coordinated to the functional groups at the surface of the Ketjen black originated from the oxidation treatment by concentrated HNO_3, while the nitrate ions are washed away. Different metal ions likely have different coordination environments, which lead to different behaviors.